ROTOR CRITICAL SPEED OF VERTICAL MOTOR EXCITED BY THE LINE FREQUENCY

Paper No. PCIC Middle-East – Al Khobar SA22_60

Lucas Selonke Klaas
WEG
Jaragua do Sul (SC)
Brazil

Abstract - Vertical motors have peculiarities regarding to the calculation of critical speed. The lower bearing, designated as a guide, has an uncertain load, which can result in a large range of bearing stiffness. The upper bearing, on the other hand, has a well-defined load. However, the bearing support stiffness varies according to the structure, in other words, it is influenced by the flange and housing geometry.

In this case, the vertical motor presented high vibration at the line frequency during the tests. The characteristics of the motor are: four poles, 60 Hz, 500 kW, and 2,300 V, and its size is: 2,066 mm height, 800 mm diameter and total mass around 3,300 kg (Fig. 1).

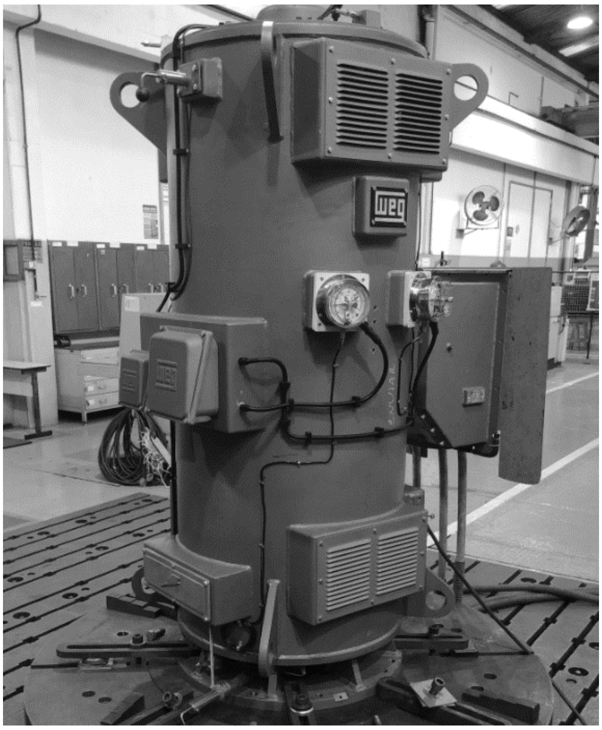

Fig. 1 – Vertical motor on the test bench.

During the theoretical evaluation, assisted by the finite element method and rotor dynamic analysis, it was found a critical rotor frequency around 58 Hz, close to the line frequency (60 Hz).

After modifying the shaft in order to increase the separation margin of the critical speed in relation to the line frequency, the motor was approved with low vibration readings.

Index Terms — vertical motor, critical speed, line frequency, vibration analysis.

I. INTRODUCTION

Vertical motors have been widely applied in the petroleum and chemical industry, more specifically in hydraulic pumps. The most common use is for water movement, as well as in chemical transport.

The main concerns about the application of vertical motors refer to the reed critical frequency, which is related to the structural stiffness (frame, brackets, and flange), mass, and position of the center of the mass. In the case of the motor and pump head assembly, the reed critical frequency is highly influenced by the pump head, since it is an important point of attention in relation to the assembly design, as evaluated in the study of influence of the attachment base [1].

Thus, it is common to carefully look at the structural analysis of the assembled machine in order to calculate the natural frequency and ensure the proper separation margin from the operating frequency as recommended in the 5th edition of the API Standard 541. The machine shall be free from structural resonance between 40 and 60% of operating speed, and the frequency ranges are defined by equation 1 [2]:

$$N = nN^* \pm 0.15N^* \tag{1}$$

N the frequency range (in Hz);
N^* the operating speed or electrical power frequency (in Hz);
n 1 and 2.

It must be noticed that the calculation method of the natural frequency for structural parts, as: frame, brackets, terminal boxes, etc., for vertical and horizontal motors is similar. However, in case of rotor dynamic analysis, there is a significant difference in the calculation for horizontal and vertical motors due to the support stiffness influence. The distribution of rotor reactions between bearings is different when compared both types of assembly. For example, for a horizontal motor, the distribution of reactions between the front and rear bearings vary according to the symmetry of the rotor in relation to the bearings. For the vertical motors, the entire weight load is applied to the thrust bearing, usually the upper bearing, while the guide bearing only receives efforts due to unbalance forces, bearing preload, magnetic force from eccentricity between the rotor and stator, or even due to misalignment between bearings or driven machine shaft end. For example, forces are reduced when compared to thrust bearing. This way, due to the reduced efforts, the bearing stiffness is low, which consequently decreases the rotor critical speed. Regarding the support stiffness, it is notable that the upper bearing is less stiff when compared to a horizontal motor.

Next topic, a way of calculating the bearing stiffness used in the rotor dynamic is presented. After that, the types of bearings for vertical motors are shown, and ahead it is clarified the difference in stiffness of the support (housing) for the upper and lower bearings. The topic V explains the electromagnetic force and how the generated forces are introduced. The topic VI presents the natural frequencies of the motor, and, finally, the last topic presents the vibration analysis of this case study.

II. STIFFNESS OF ROLLING BEARINGS

To determine the critical speed of a rotor, it is necessary to calculate a complex system with numerous degrees of freedom that involves, beyond the rotor, the bearings, and the bearing supports. As mentioned by Gargiulo [3], bearings play a vital role in the dynamic behavior of the rotor system since the bearing deflects when subjected to loads. To calculate bearing stiffness, simplified models are used, considering the geometry and direction of the load and variations between radial and axial. For deep-grove or angular-contact bearings that are commonly applied in vertical motors, it is possible to apply the equations 2 and 3 [3].

$$K_r = 1.88 * 10^3 * \sqrt[3]{DF_r Z^2 cos^5 \propto} \qquad (2)$$

$$K_a = 3.43 * 10^3 * \sqrt[3]{DF_a Z^2 sin^2 \propto} \qquad (3)$$

In which:

K_r	radial bearing stiffness (N/mm);
K_a	axial bearing stiffness (N/mm);
D	rolling elementer diameter (mm);
F_r	radial external force (N);
F_a	axial external force (N);
Z	number of rolling element;
$\propto$	contact angle (rad).

The ratio of bearing stiffness to shaft stiffness has a significant impact on the critical speed and on the associated mode shape [4]. This effect will be further explored, in the case study.

Bearing stiffness is characterized by the elastic deformation of the ball under load (Fig. 2) and depends not only on the bearing type, but also on the bearing size, and the mounting tolerances during operation. Thus, stiffness can be increased by increasing the preload [4].

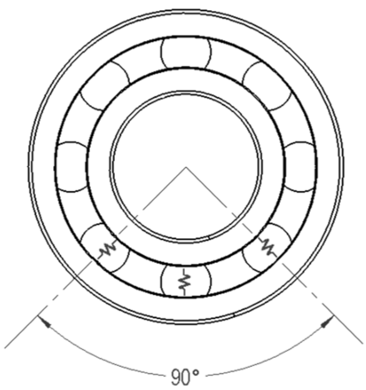

Fig. 2 – Bearing load area for horizontal motor.

The calculated bearing stiffness for the guide bearing of the analyzed motor is 2.47E+06 N/m, and for the thrust bearing is 2.76E+08 N/m, considering the spring load, and the rotor weight, respectively. There is a great difference of stiffness mainly influenced by the bearing load.

Fig. 3 shows the undamped critical speed map for this rotor as a function of the stiffness of the bearings. The abscissa denotes the stiffness of the bearing, while the ordinate is the critical speed of the rotor. It was added two horizontal lines: the rotational speed (1,800 rpm), and the line frequency (60 Hz = 3,600 rpm).

This plot highlights the closeness of the line frequency to the first critical speed. This diagram is useful to analyze the critical speed behavior with bearing stiffness variations. The mode around 60 Hz presents flexible body behavior and rigid support.

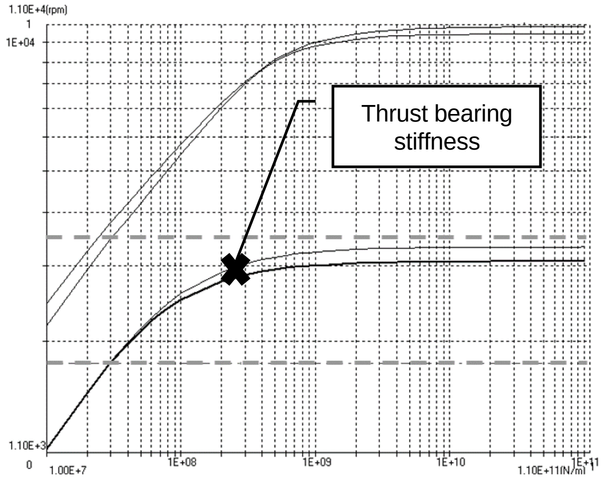

Fig. 3 – Critical speed map.

III. TYPES OF BEARINGS FOR VERTICAL MOTORS

There are two types of bearings widely used in motors: rolling, and sliding. Recently, it has been observed the use of magnetic bearing for electric motors in high-speed application [5]. In this article, only rolling bearings are considered, with emphasis on bearings applied in vertical motors, without evaluating the lubrication requirements, whether by grease or oil bath.

The load applied to the bearings depends on the efforts at the drive end shaft. For example, in the case of a pulley, it will cause a high radial load on the guide bearing. Or, in case of high axial thrust, the mechanical designer can change the conventional arrangement of bearings using the lower bearing as the thruster bearing.

Excluding special cases, in most of the vertical motor applications, the lower bearing is the guide, and the upper bearing is the thrust (Fig. 4).

For a correct understanding, the function of each bearing is explained. The thrust bearing is responsible for receiving the axial forces. Thus, all the weight force will be applied to this bearing and also axial thrusts of the application, if there is any. Angular contact ball or roller bearings are generally selected for thrust bearings due to the high loads.

For the guide bearing keeps the rotor aligned at vertical position and receives unbalanced loads of the rotor, due to the reduced radial loads, is usually applied ball bearing. The bearing is free to slide over the hub to accommodate the shaft thermal expansion. Therefore, hub tolerances should not influence bearing stiffness. For example, it will rarely design an interference fit between bearing and hub. Otherwise, the guide bearing will not slide during the thermal shaft expansion, instead of the guide bearing going down, the thrust bearing will come loose during operation causing high vibration and damage.

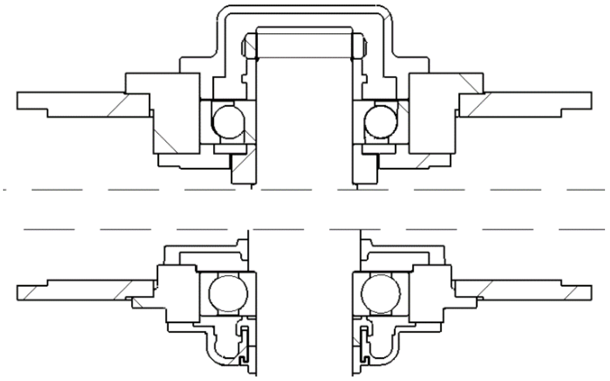

Fig. 4 – Vertical motor typical bearings arrangement.

IV. SUPPORT STIFFNESS

As already mentioned, the housing will influence the dynamic of rotor as it is an integral part of the analysis, added as the support stiffness and mass. About this point, the difference between a vertical and a horizontal motor is clear. The thrust support has lower stiffness compared to the guide, and the difference becomes even higher as the distance between bearings increases. As a result, the motor gets longer.

In order to a quantitative evaluation, a numerical analysis was performed to obtain the support stiffness for the guide and thrust bearings. On the left side of the Fig. 5, the deformation of the support for the guide bearing is shown, while on the right side of the same figure it is possible to see the deformation of the support for the thrust bearing. The forces were applied at horizontal direction (z-axis). For the guide bearing, the deformation is directly influenced by the flange that connects the frame to another equipment, usually the pump head. The deformation of the thrust bearing is directly related to the housing design.

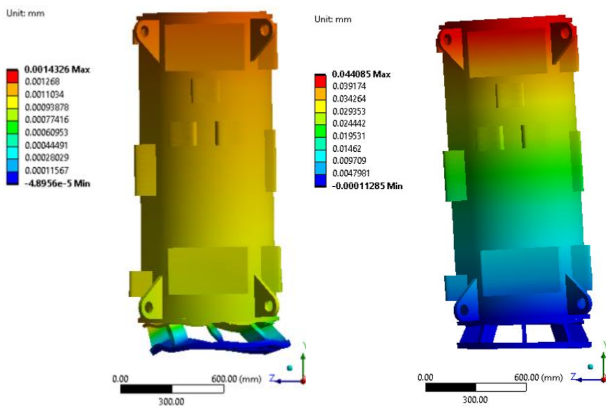

Fig. 5 – Deformation of frame according to the bearing forces. The left side represents forces on the guide bearing, and the right one, the forces on the thrust bearing.

The obtained thrust bearing support stiffness is 2.27E+07 N/m, while for the guide bearing it is 6.98E+07 N/m. Thus, the support for the thrust bearing is 68% less stiff.

The equivalent stiffness is the result of the series stiffness of the bearing and support, as shown in equation 4. The calculated equivalent stiffness for the thrust bearing is 2.10E+07 N/m, showing the influences of the support by the reduction of the stiffness in comparison to the bearing stiffness. On the other hand, for the guide bearing, the equivalent stiffness is 2.38E+06 N/m, similarly to the bearing stiffness. In summary, the equivalent stiffness is governed by the lowest series stiffness.

$$\frac{1}{k_{eq}} = \frac{1}{k_b} + \frac{1}{k_s} \tag{4}$$

In which:

k_{eq} equivalent stiffness (N/m);
k_b bearing stiffness (N/m);
k_s support stiffness (N/m).

V. LINE FREQUENCY EXCITATION

Considering the perfectly circular rotor, with all electrical properties symmetrical to the axis of rotation, centered on a stator also perfectly circular, it leads to no radial resultant force between rotor and stator in operation with current, voltage, and rotation at rated condition. The Fig. 6 shows the flux lines based on previous considerations. However, it is difficult to obtain perfect symmetry during the manufacture of an electric motor due to the precision of the manufacturing machines, as, for example, the tool responsible for stamping the lamination, the machining of the shaft and brackets, and also due to the assembly tolerances.

Even in healthy motors, there is an asymmetry in the air gap that generates an inhomogeneous distribution of the flux lines responsible for the creation of radial forces, also called unbalanced magnetic pull, which act on the air gap and are proportional to the voltage applied to the stator.

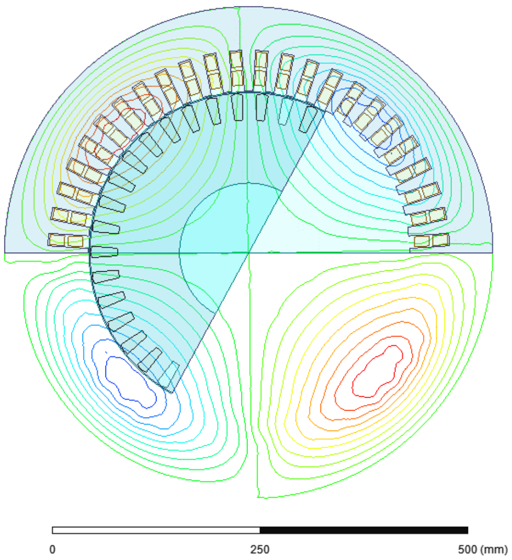

Fig. 6 – Flux lines between rotor and stator.

The asymmetry on the air gap can be static, dynamic, or both. The static eccentricity occurs when the rotor axis of rotation coincides with the rotor symmetry centerline, but they do not coincide with the stator axis of symmetry. The dynamic eccentricity occurs when the rotation axis does not coincide with the rotor symmetry axis, but it is coincident with stator centerline. When the rotation axis does not coincide with either the rotor symmetry axis or the stator symmetry axis, there is a combined static and dynamic eccentricity condition of the air gap.

In horizontal motors, unlike vertical motors, there is often an intrinsic static eccentricity due to gravity acting on the rotor generating displacement, also known as static elastic line. In vertical motors, the gravity acts in the axial direction, not influencing the eccentricity.

Lateral magnetic forces are generated due to air gap eccentricity and expressed as Maxwell's stress equation (eq. 5) [6]. It can be said that the magnetic force is proportional to the square of flux density in the airgap.

$$F = \frac{B_g^2}{2\mu_0} S \tag{5}$$

In which:

B_g^2	flux density;
μ_0	permeability of free space;
S	air gap area.

The unbalanced magnetic pull forces for static eccentricity of the air gap occurs at the frequency of twice line frequency. The excitation of the line frequency only occurs when there is dynamic or mixed eccentricity or the air gap.

Generally, 10% of static eccentricity is often acceptable for a healthy motor. Usually, trying to reduce the eccentricity level as much as possible (to under 5%) to reduce the unbalanced magnetic pull minimizes the vibrations and noise [7]. Dynamic eccentricity should be as low as possible.

In order to evaluate the forces involved, a simulation was performed showing with 10% eccentricity in the air gap. The unbalance magnetic pull results in 2,300 N for this eccentricity condition.

VI. NATURAL FREQUENCIES

The rotor under analysis is shown in Figure 8. The motor is asynchronous with a cast aluminum squirrel cage.

Fig. 8 – Rotor.

Along with the analysis of critical speed, it was analyzed the natural frequencies of the static part.

The Coriolis effect due to rotation was considered in the rotor analysis. Figure 7 presents the Campbell diagram for the assembled machine with the first natural frequency (reed frequency). It is possible to observe the interference of the 1X rotation and 2X rotation sloping lines. The line frequency is the same of 2X rotation (60 Hz). The vertical dashed line is the 1X rotation (1,800 rpm).

For the finite element method for geometric modeling, both the inertia flywheel and the rotor were considered as masses. They were not considered stiffening effects.

In the Campbell diagram (Fig. 7), it is possible to notice, during acceleration, up to the nominal speed (1,800 rpm), 1X rotation interferences at 10 and 25 Hz. The vibration mode at 10 Hz (Fig. 9) is influenced by the low stiffness of the guide bearing. At 25 Hz, the reed critical frequency is observed (Fig. 10). As it can be seen, the deviation from the rated speed is 20% considering the motor on a rigid basis. After fixing the motor on the pump head, the reed critical frequency will be reduced, and there will be a greater separation margin from the rated speed.

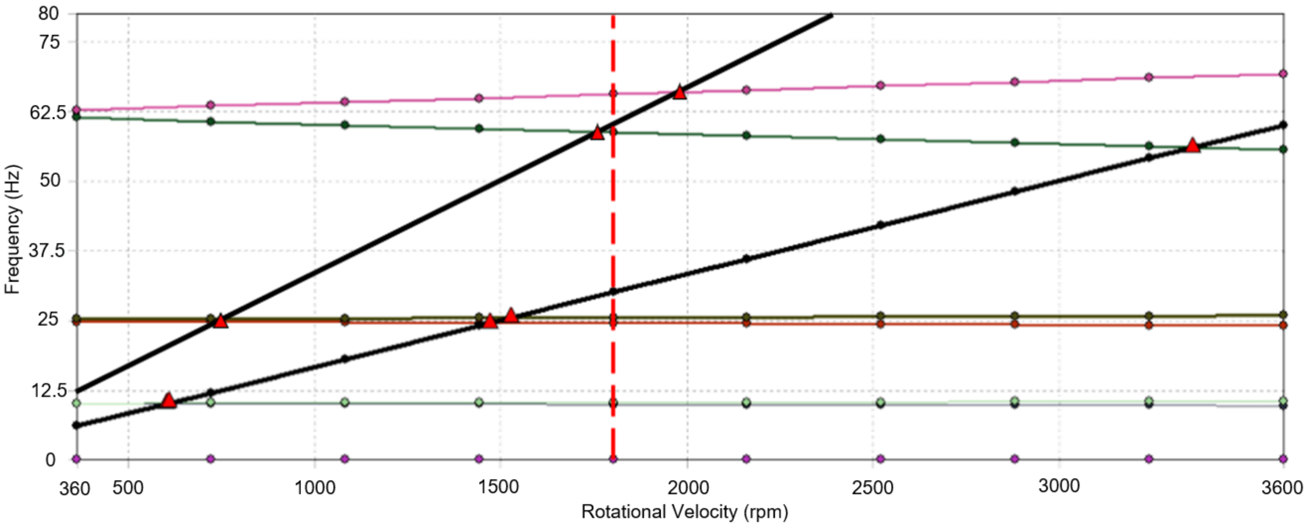

Fig. 7 – Campbell diagram.

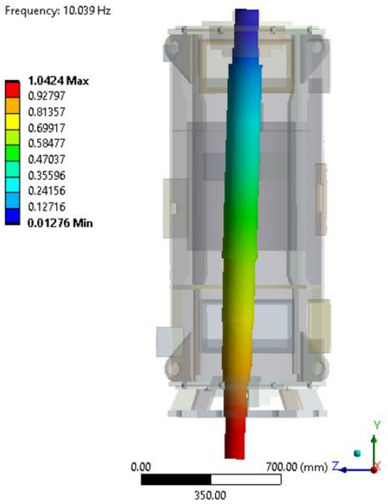

Fig. 9 – First rotor critical speed.

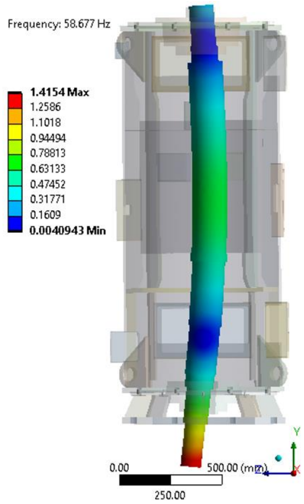

Fig. 12 – Second critical speed.

For the second rotor critical speed, it is observed that the shaft end has a greater displacement (Fig. 12). The rotor lamination is also influenced by this mode of vibrating in phase opposition at the shaft end, similarly to a bow shape. As it can be seen in Figure 12, there is no displacement in the thrust bearing, but there is substantial displacement in the guide bearing, showing the influence of stiffness on the shape mode.

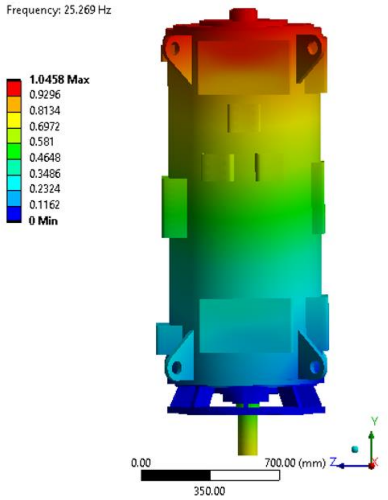

Fig. 10 – Reed critical frequency.

A harmonic analysis was performed applying the same amplitude force in the rotor along with the entire frequency range from 0 to 80 Hz. Figure 11 shows the response for the thrust bearing position. The reed critical frequency response (4.4 mm/s) highlights in comparison to the critical speed (1.5 mm/s).

VII. VIBRATION ANALYSIS

At the first vibration test, the vibration amplitude was above the specified according to IEC 60034-14 [8]. The fast-Fourier transform (FFT) spectrum analysis (Fig. 15) showed high vibration at 1X and 2X rotation speed. As it is a vertical motor fixed to the test base, it is common to check the natural frequencies. The experimental method used to determine the natural frequencies is through the bump test. The motor was impacted on the upper part of the housing, and the response was measured. Natural frequencies at 23, 59.5 and 96 Hz were observed (Fig. 14).

In this test, it was not possible to observe the critical speed of the rotor at 10 Hz. The natural frequency at 23 Hz is related to the reed critical frequency. The calculated reed frequency was 25 Hz for the motor fixed to a rigid and massive base. However, due to the influence of the fixation base, the natural frequency reduces.

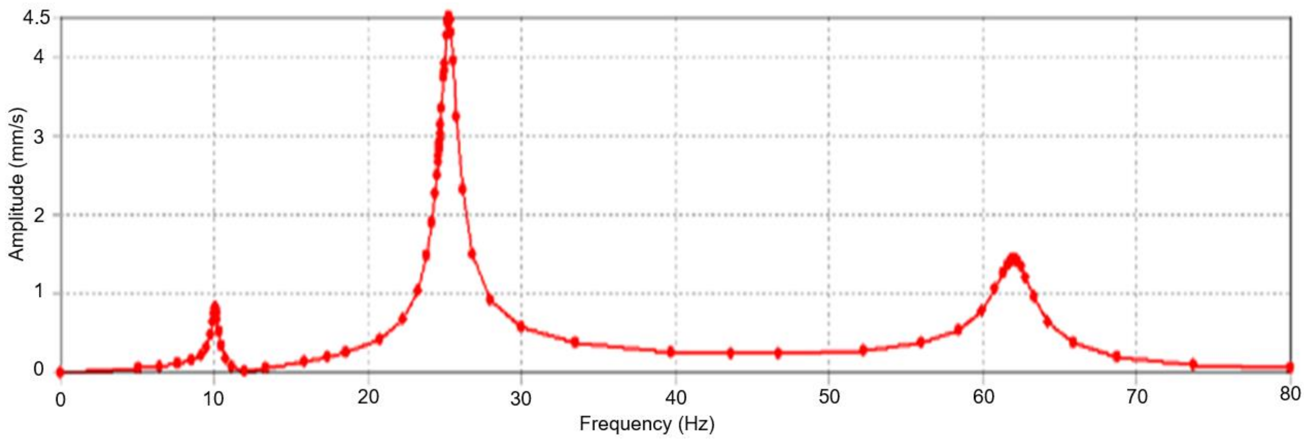

Fig. 11 – Harmonic response.

The natural frequency at 59.5 Hz is relative to the rotor without the influence of rotation speed, as the measurement was carried out in a static condition. Finally, 96 Hz is the natural axial frequency of the motor, as identified in Fig. 13.

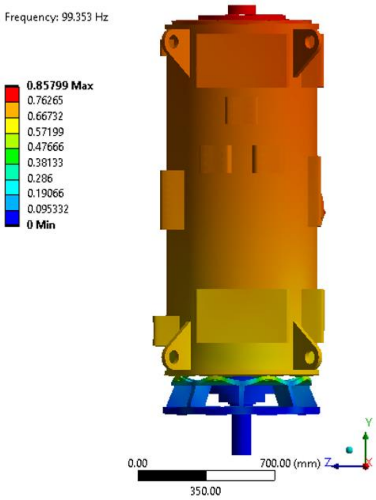

Fig. 13 – Axial mode of the motor.

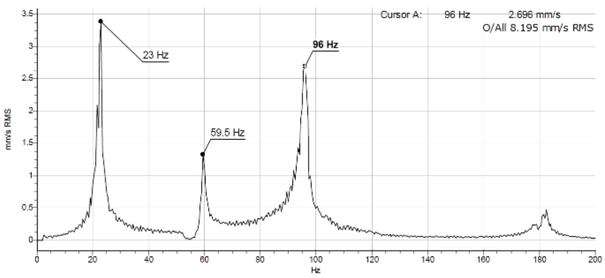

Fig. 14 – Bump test at upper bearing.

Regarding the initial FFT spectrum, it was possible to observe the influence of the voltage applied to the stator. With the nominal voltage, it was measured 1.4 mm/s rms at 60 Hz (Fig. 15). By reducing the voltage applied to the half, the vibration reduces to 0.3 mm/s rms, showing high influence of the magnetic force (Fig. 16).

After initial measurements, the rotor was balanced in two planes. The vibration at 30 Hz was reduced, remaining a higher component at 60 Hz (Fig. 18). This behavior is a characteristic of the dynamic eccentricity.

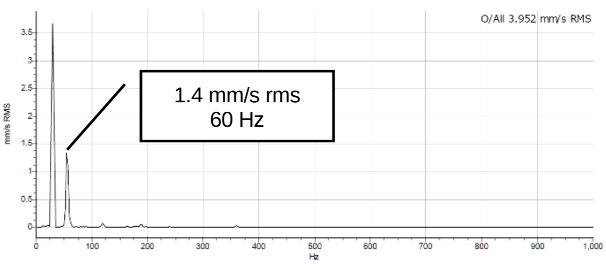

Fig. 15 – Spectrum of thrust bearing with rated voltage.

It can be understood that the balance correction mass reduced the eccentricity of the rotor in relation to the rotation axis (Fig. 17) reducing the amplitude at 1X.

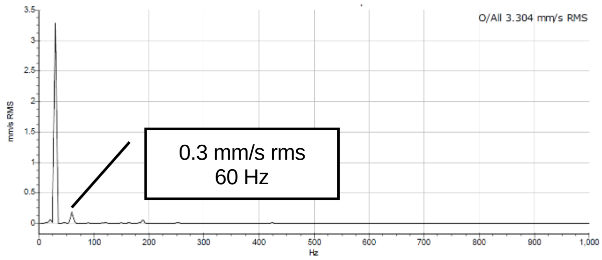

Fig. 16 – Spectrum of thrust bearing with reduced voltage.

However, the addition of the mass causes the dynamic airgap eccentricity, thus increasing the magnetic pull force, which consequently means greater excitation of resonance resulting in the increase of 2X vibration amplitude.

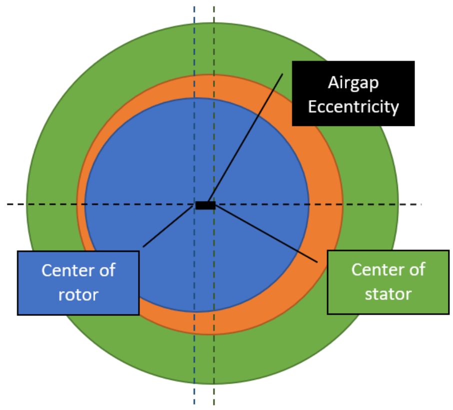

Fig. 17 – Rotor rotating around its center of mass, but eccentric regarding the stator.

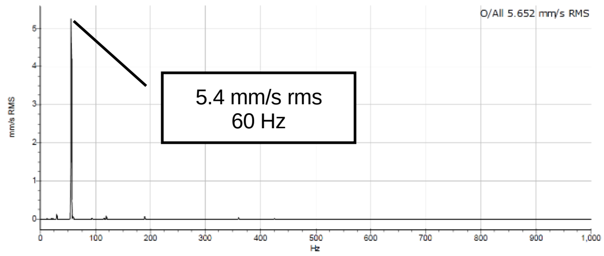

Fig. 18 – Spectrum of thrust bearing after balancing.

Through the analysis of the natural frequencies, along with the balancing response and due to the change in vibration with the variation of the stator voltage, it was decided to move the critical speed through shaft machining. The others options would be:

- to increase the guide bearing stiffness by increasing the bearing preload, but this option is not feasible. Firstly, due to the quantity of springs needed to increase and secondly due to the increase in load on the thrust bearing;
- correct the rotor dynamic eccentricity. However, this task is not simple since it is not related only to the geometric dimensions. There may also be magnetic influence, which is related to the properties of the cast rotor and coils.

As a complementary test, the vibration was evaluated at two additional electrical frequencies. The magnetic flux was kept the same by adjusting voltage to the line frequency. In both cases, there was reduction in the vibration amplitude measured in velocity (mm/s rms). Table 1 shows the comparison.

Table 1 – Vibration levels according to frequency.

mm/s rms	Guide bearing			Thrust bearing		
Condition (Hz)	Horizontal	Vertical	Axial	Horizontal	Vertical	Axial
55	0.18	0.25	0.30	0.39	0.37	0.32
60	0.37	0.88	2.19	5.65	4.65	1.62
63	0.19	0.24	0.46	1.83	1.69	0.36

After evidence of the resonance, the shaft diameter next to the laminated sheets was machined according to Fig. 19. The diameter close to the guide bearing was reduced by 20 mm, and the diameter close to the thrust bearing by 30 mm. The original diameters were 170 and 160 mm respectively, and now they are 140 mm for both cases.

This diameter reduction has no changes to safety factor of torsional and bending stress once the end shaft diameter is 100 mm with a keyway depth of 10 mm. The critical speed shift from 59.5 to 56 Hz provides margin of 4 Hz in relation to the line frequency (or 2X rotation).

Fig. 19 – Indication of shaft machining in red.

VIII. CONCLUSIONS

According to the evaluation of the natural frequencies, the match between the critical speed with 2X rotation or the line frequency was observed, which resulted in excitation of the first flexible body mode of the rotor.

Due to inaccuracy of guide bearing stiffness, in which the radial loads are uncertain, imprecision of the calculated critical speed was caused.

The defined load of the guide bearing are the preload springs, which in turn created the minimum load on the bearing, representing 10% of the maximum load. That is, it promotes low deformation and stiffness, directly affecting the reduction of the critical speed.

After modifying the shaft by reducing the diameter, the vibration levels were below the standard limit, showing no significant variation between the cold and hot conditions, as shown in Table 2.

Fig. 20 presents the critical speed map in comparison to Fig. 3. The curve of the first critical speed decreased to the previous condition.

Table 2 – Final vibration after shaft machining.

mm/s rms	Guide bearing			Thrust bearing		
Condition	Horizontal	Vertical	Axial	Horizontal	Vertical	Axial
Cold	0.37	030	0.48	1.25	1.40	0.45
Hot	0.27	0.58	0.33	1.28	1.35	0.39

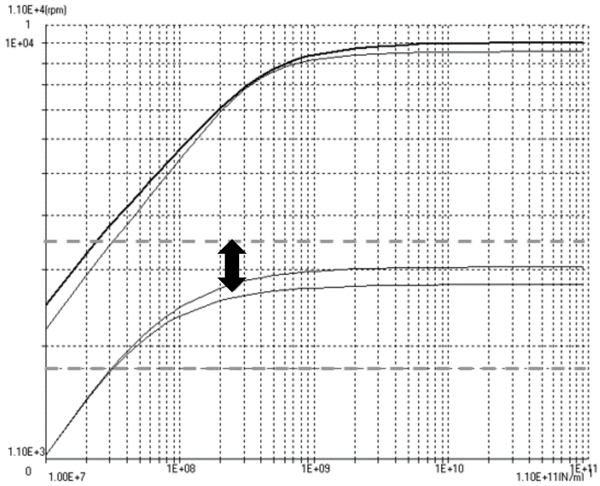

Fig. 20 – Critical speed map after modification.

In summary, due to the difficulty of determining the stiffness of the guide bearing, it is recommended to evaluate the lateral analysis of the rotor through the critical speed map in order to obtain appropriate separation margin in relation to 1X and 2X rotation frequency and also 1X line frequency.

IX. REFERENCES

[1] Goncalves, V. S., Silva, H. P., & Schiochet, E. (2016). Study of the test base influence on the electric motor reed critical frequency. Petroleum and Chemical Industry Conference Europe Conference Proceedings, PCIC EUROPE, 2016-Octob. https://doi.org/10.1109/PCICEurope.2016.7604639

[2] API 541 5th edition: Form-Wound Squirrel Cage Induction Motors – 375kW (500 HP) and Larger 541, A., & Edition, F. (2003). Form-Wound Squirrel Cage Induction Motors - 250 Horsepower and Larger. *Policy*, *April*.

[3] EP Gargiulo Jr, A simple way to estimate bearing stiffness, Machine Design, January 1980.

[4] Swanson, E., Hill, C., Carolina, N., Powell, CD, Corporation, ST, Weissman, S., Wasserman, A., & Caldwell, W. (2005). *A Practical Review of Rotating Machinery Critical Speeds and Modes*. *May*, 10–17.

[5] Eaton, D., Rama, J., & Singhal, S. (2010). Magnetic bearing applications & economics. Record of Conference Papers - Annual Petroleum and Chemical Industry Conference. https://doi.org/10.1109/PCIC.2010.5666819

[6] Chiba, A. (n.d.). 02 Electromagnetics and mathematical model of magnetic bearings. In Magnetic Bearings and Bearingless Drives. Akira Chiba, Tadashi Fukao, Osamu Ichikawa, Masahide Oshima, Masatsugu Takemoto and David G. Dorrell. https://doi.org/10.1016/B978-0-7506-5727-3.50005-5

[7] Salah, AA, Dorrell, DG, & Guo, Y. (2019). A review of the monitoring and damping unbalanced magnetic pull in induction machines due to rotor eccentricity. *IEEE*

Transactions on Industry Applications, *55* (3), 2569–2580. https://doi.org/10.1109/TIA.2019.2892359

[8] International Electrotechnical Commission – IEC 60034 Rotating Electrical Machines Part 14: Mechanical Vibration of Certain Machines with Shaft Heights 56 mm and Higher – Measurement, Evaluation and Limits of Vibration Severity – Standard, Geneva, 2007.

X. VITA

Lucas Selonke Klaas received his B.S. and M.S. degree in mechanical engineering and science and engineering of materials from the State University of Santa Catarina, Brazil, in 2007 and 2013, respectively. Currently, he is doing a doctorate in electrical engineering. His research interest is bearingless motor. He is a design engineer and vibration specialist of WEG Energy since 2008. E-mail: lucask@weg.net